A systematic study of the oxygen K edge in the cubic and less common monoclinic phases of the rare earth oxides (Ho, Er, Tm, Yb) by electron energy loss spectroscopy

2006 J. Phys.: Condens. Matter 18 2181

(http://iopscience.iop.org/0953-8984/18/7/007)

INSTITUTE OF PHYSICS PUBLISHING JOURNAL OF PHYSICS: CONDENSED MATTER

J. Phys.: Condens. Matter **18** (2006) 2181–2189 doi:10.1088/0953-8984/18/7/007

A systematic study of the oxygen K edge in the cubic and less common monoclinic phases of the rare earth oxides (Ho, Er, Tm, Yb) by electron energy loss spectroscopy

Ashley Harvey[1], **Bing Guo**[2], **Ian Kennedy**[2], **Subhash Risbud**[1] **and Valerie Leppert**[3,4]

[1] Department of Chemical Engineering and Materials Science, University of California, Davis, CA 95616, USA
[2] Department of Mechanical and Aeronautical Engineering, University of California, Davis, CA 95616, USA
[3] School of Engineering, University of California, Merced, CA 95344, USA

E-mail: vleppert@ucmerced.edu

Received 16 November 2005, in final form 12 January 2006
Published 2 February 2006
Online at stacks.iop.org/JPhysCM/18/2181

Abstract

Transmission electron microscopy and electron energy loss spectroscopy (EELS) were used to distinguish structural details for the cubic and uncommon monoclinic crystal phases of heavy metal rare earth oxide nanoparticles synthesized by a combustion process. Specifically, we systematically examined the EELS oxygen K edge for Ho, Tm, Er, and Yb sesquioxides in both phases. This work presents, to our knowledge, the first EELS study of the monoclinic phase in these materials and the first systematic comparative study between the monoclinic and cubic phases across a range of rare earth sesquioxides. For both phases, we observed the usual double-peak structure of the oxygen K edge typically seen for oxygen atoms tetrahedrally surrounded by metal atoms, but we found the details of the energy loss near-edge structure to differ substantially between the two phases. Our results indicate a greater peak separation for the cubic than for the monoclinic phase. Furthermore, a trend of increasing peak separation with increasing atomic number was also noted for both phases in the series of rare earth oxide nanoparticles. Our results show that the fine structure in EELS can be utilized to determine differences on the nanoscale between the common cubic structure and the less common monoclinic structure.

[4] Author to whom any correspondence should be addressed.

1. Introduction

Rare earth oxide (REO) thin films and nanoparticles (NPs) have been investigated recently for many applications including optical devices [1] and dielectric [2, 3] and catalytic [4, 5] materials. REO materials are generally known for their ability to emit visible to infrared light, as well as their high dielectric constant and refractory nature. In some instances, the structure of the oxide may change the physical properties observed, such as photoluminescence and conductivity. Determining the chemical composition and the structure of REO materials at the nanoscale is essential for complete characterization.

Rare earth sesquioxides (RE_2O_3) are known to form three different phases at atmospheric pressure, depending on the metal's ionic radius. For La to Nd the hexagonal phase ($P32/m$) is most commonly formed, while for Pm to Dy the cubic phase ($Ia3$) is formed at lower temperatures and the monoclinic phase ($C2/m$) may be formed at elevated temperatures. For Ho to Lu only the cubic phase is formed at atmospheric pressure, but Hoekstra has shown that the monoclinic phase can be attained in bulk materials with a high pressure technique [6]. We have recently synthesized NPs of the heavy rare earth oxides (Ho to Yb) and yttrium oxide in the monoclinic phase at atmospheric pressure with a gas-phase combustion process [7]. These novel materials are ideal candidates for a systematic comparison of the cubic and monoclinic phases across a range of rare earth oxides.

Electron energy loss spectroscopy (EELS) is a component of transmission electron microscopy (TEM) that has recently been exploited to study the electronic structure and atomic bonding of many different materials [8]. It has been shown that for many transition metal oxides (TMOs) the oxidation state of the cation as well as the crystal structure can affect the fine structure of the oxygen K edge [9–11]. Some EELS studies have been done on REO materials, though not as many as for TMO materials, and most focus on identifying the oxidation state of a multivalent species, especially cerium, in oxides or glasses based on the fine structure of the rare earth M (3d) ionization edge and, in particular, the ratio of the M_5 to M_4 lines [12–14]. There are some systematic EELS studies of the RE sesquioxides as a group, for example by Manoubi *et al* [15], Brown *et al* [16], and Fortner and Buck [17]. In these, the RE $M_{4,5}$ white lines, representing electronic transitions from the 3d level to unoccupied f orbitals, were described in terms of the variation of their width, separation, and splitting in relation to the RE atomic number. A trend was established, showing that the M_5/M_4 ratio increases with atomic number as the filling of the 4f shell increases, going towards the end of the series, where the M_4 line disappears. Brown *et al* [16] also reported that the oxygen K-edge shape depends mostly on the crystal structure, with the edge having a double peak for the cubic structure and a broad rounded peak for the monoclinic. This last statement was later revised [18] to describe the splitting of the double-peak shape in the edge as simply more pronounced for the cubic structure than for the monoclinic.

In the present study, we show that the shape of the oxygen K edge and the energy difference between the two peaks observed in the EELS spectrum fine structure can be used to differentiate the cubic structure from the monoclinic in heavy RE_2O_3 NPs. We also show that, within the group of heavy REO samples we have examined, there is a trend in the degree of separation between the two oxygen K-edge peaks with respect to the RE ionic radii or atomic number.

2. Experiment and data analysis

Nanoparticulate powders of Ho_2O_3, Er_2O_3, Tm_2O_3, and Yb_2O_3 were synthesized with a gas-phase combustion technique detailed elsewhere [7]. Briefly, RE beta-diketonate precursors—tris(2,2,6,6-tetramethyl-3,5-heptanedionato) RE(III)—were placed in a stainless steel basket

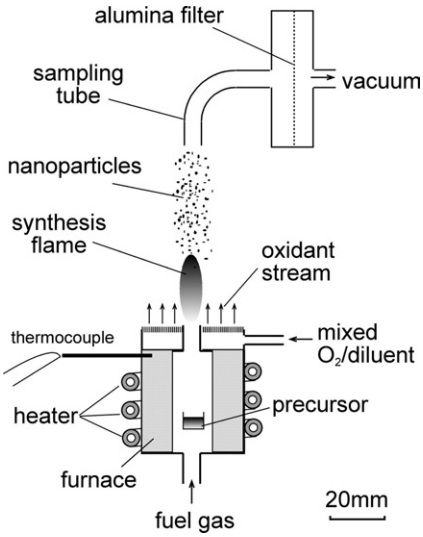

Figure 1. Set-up used for the combustion synthesis of the REO-NPs. The fuel gas was hydrogen and the supporting gas was either pure oxygen or oxygen mixed with nitrogen to regulate the flame temperature.

that was heated in a stainless steel furnace to generate the vapour of the precursor. Hydrogen fuel gas carried the vapour and together they flowed through a nozzle to ignite and form an H_2 diffusion flame in a gas co-flow at atmospheric pressure. The supporting gas co-flow was composed of N_2 and/or O_2. In the flame, the precursor vapour decomposed to form the lanthanide sesquioxide, which formed nanoparticles that were collected on an alumina membrane filter. The flame temperature was adjusted by changing the ratio of N_2 to O_2. In figure 1 is a schematic diagram of the synthesis set-up.

X-ray diffraction (XRD) patterns were obtained on a Scintag PAD V x-ray diffractometer with Cu Kα radiation. To prepare the XRD sample, a piece of the alumina filter bearing a thin layer of RE_2O_3 nanoparticles was carefully cut and mounted on a glass substrate. The XRD patterns were analysed using the MDI JADE 6.0 program.

Transmission electron microscopy (TEM) samples were prepared by suspending the REO-NPs in ethanol, sonicating the solution for 30 s to break up large agglomerates, and then dispersing one drop of the solution on a holey carbon-filmed TEM grid. A Philips CM-200 TEM was used for EELS with a field emission gun operated at 197 kV (200 kV minus 3 kV while the GIF was in operation), producing a beam with an energy spread of about 0.9 eV at the FWHM of the zero-loss peak (ZLP). EELS measurements were carried out in TEM image mode with the beam condensed to probe only a few particles at one time, and EELS spectra were collected on a Gatan image filter (GIF) with a dispersion of 0.1 eV per channel. Short acquisition times (1.5–3 s) were used to minimize effects related to energy drift in the source such as peak broadening, and several spectra from the same area were summed to improve the signal-to-noise ratio for the quantitative calculations. The selected area electron diffraction (SAED) patterns and images of the NPs as well as the EELS spectra were monitored to ensure that the samples did not undergo transformation in the electron beam. Conventional TEM images were obtained on a Philips CM-12 operating at 100 kV with a LaB_6 thermionic source.

Digital Micrograph (DM) software was used for background removal by a power-law curve fit (AE^{-r}) below the O K edge, as is standard [8]. DM was also used to smooth the data with a

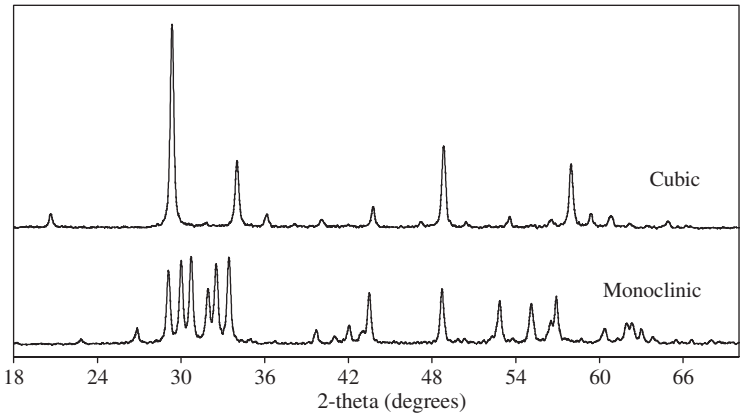

Figure 2. Representative XRD patterns of cubic (top) and monoclinic (bottom) Er_2O_3. XRD patterns were taken for all of the RE_2O_3 compositions, with similar results. The Er_2O_3 cubic pattern matched PDF #08-0050 for cubic Er_2O_3, and since there was no record of the monoclinic phase for the heavy RE_2O_3 compositions in the JC-PDS database CaRIne software was used to construct the unit cell and simulate an XRD pattern, which matched the experimental pattern well.

1 eV window in order to improve the signal-to-noise ratio and minimize anomalous artifacts in the spectra. No material was added to the TEM sample for an internal calibration of the energy loss scale, so the spectra were aligned to each other by setting the maximum of the first peak on the oxygen K edge to 532 eV. The low-loss region of the spectrum was recorded for each area examined, and the data chosen for analysis were those with a sample thickness less than half of the electron inelastic mean free path. The particles were thin enough so that sampling them individually should not have caused plural scattering effects, but even when there were multiple particles sampled at one time the first plasmon peak in the low-loss spectrum lies approximately 15–20 eV above the ZLP, and so will not interfere with the analysis of the energy loss near-edge structure (ELNES) that is evaluated here.

After adding several spectra together, Pearson's method [19] was followed to model the contributions of continuum transitions to the oxygen K edge. A straight line was drawn from the edge onset to where the falling edge of the second peak intersected the background signal, and this was subtracted from the data. The two peaks remaining in the ELNES were then modelled with Lorentzian curves to determine the energy loss at which the peak maxima occurred. This technique is valid here because our quantitative analysis is concerned only with the relative energy loss values of the peaks and not the peak intensity.

3. Results

As determined with XRD, all of the RE_2O_3 samples synthesized at a low flame temperature (where $N_2/O_2 = 3.76$) were in the common cubic phase. The RE_2O_3 samples synthesized at a high flame temperature (pure O_2 as the co-flow gas) invariably had the monoclinic structure. Neither the higher- nor the lower-temperature synthesis ever produced a mixture of the two phases. Two XRD patterns are shown in figure 2 to demonstrate each crystal structure. The grain size of the RE_2O_3 samples, as determined from whole-pattern fitting and Rietveld refinement of the XRD data, ranged from approximately 20 to 50 nm. The grain size measured by XRD was in reasonable agreement with the particle size indicated by TEM as shown in the images of representative samples seen in figure 3, where (a) shows the cubic NPs, and

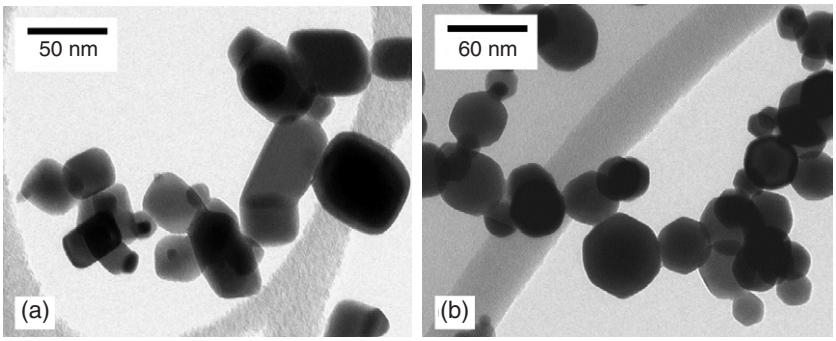

Figure 3. TEM bright-field images of cubic (a) and monoclinic (b) Er_2O_3. The NP size range was approximately 20–60 nm, and the NP projections in the images show morphologies that correspond with each crystal structure.

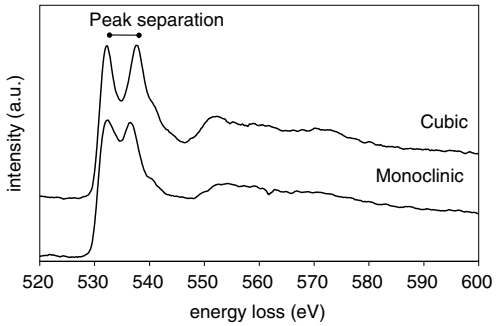

Figure 4. EELS spectra of cubic (top) and monoclinic (bottom) Er_2O_3, showing the difference in oxygen K-edge ELNES. The separation between the two peaks is greater for the cubic phase versus the monoclinic, and the peaks appear to overlap more in the monoclinic phase.

(b) shows the monoclinic. There was significant morphological difference between the particles of the cubic and monoclinic structures. Most cubic phase particles have rectangular projections in the TEM micrograph while the particles with the monoclinic structure have somewhat hexagonal projections, in accordance with their respective crystal structures and indicating that the particles are each single crystals. A discussion of the formation of the REO-NPs in both phases can be found in [7].

Typical EELS spectra collected from each phase are presented in figure 4. The spectrum of the cubic RE_2O_3 NPs shows two peaks that are clearly separated and occur within about 5 eV of the O K edge. In the EELS spectrum of the monoclinic NPs, the two peaks are still evident, but the peak separation is not as great and the difference between the minimum separating the peaks and the maxima of the peaks is not as large as in the cubic phase; the peaks appear to overlap more in the monoclinic instance.

Quantitatively, the mean peak separation for the cubic phase ranges from 5.37 eV for Ho_2O_3 to 5.58 eV for Yb_2O_3, and that for the monoclinic phase ranges from 4.03 eV for Ho_2O_3 to 4.57 eV for Yb_2O_3 as detailed in table 1. On average, there is a difference in peak separation of 1.18 eV between the cubic and monoclinic phases. For the cubic phase, there is a difference of 0.21 eV between the heaviest and lightest RE oxides, while for the monoclinic this difference is 0.54 eV.

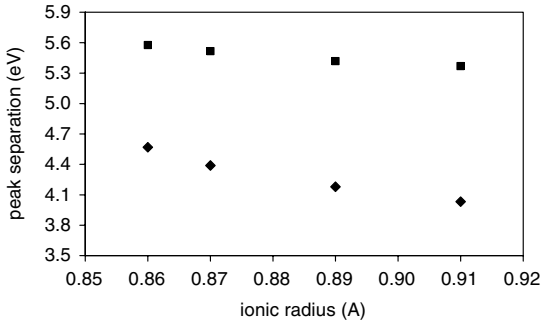

Figure 5. Graphical comparison of the oxygen K-edge peak separation based on the crystal structure and cationic radius (atomic number). The separation of the peaks is always less for the monoclinic NPs versus the cubic, and as the ionic radius increases (atomic number decreases) the peak separation decreases.

Table 1. The values of peak separation in the oxygen K-edge EELS fine structure found for each heavy RE_2O_3 in the cubic and monoclinic phases.

			Mean peak separation (eV)	
Oxide	Atomic No	Ionic radius (Å)	Monoclinic	Cubic
Ho	66	0.91	4.03 ± 0.06	5.37 ± 0.11
Er	67	0.89	4.18 ± 0.08	5.42 ± 0.03
Tm	68	0.87	4.39 ± 0.19	5.52 ± 0.07
Yb	69	0.86	4.57 ± 0.09	5.58 ± 0.09

Two trends are observed.

(1) The peak separation here is always less for the monoclinic phase than the cubic.
(2) With increasing atomic number and decreasing ionic radius the peak separation increases slightly.

These trends are shown graphically in figure 5.

4. Discussion

As with all core-loss edges accessible in EELS and x-ray absorption spectroscopy (XAS), the oxygen K-edge shape is influenced by several factors including the ejection of electrons into the continuum, producing a saw-tooth shape, as well as solid state effects and transitions to unoccupied bound states, which can create fine structure in the edge [20].

It has been reported that for dioxides of cerium (a light rare earth), titanium, zirconium, and uranium, the ELNES (or equivalent x-ray absorption near-edge structure, XANES) of the oxygen K edge is due to the crystal field splitting of the metallic d orbitals into e_g and t_{2g} components, resulting in the EELS double-peak signature of tetrahedrally coordinated oxygen atoms [10, 13, 21–23]. This theory is based on the molecular orbital (MO) model, in which the d orbitals of the metal are hybridized with the p orbitals of the oxygen atom. McComb specifically investigated the ELNES of the oxygen K edge of three zirconia pseudopolymorphs: monoclinic, cubic stabilized, and tetragonal stabilized ZrO_2, as a method to circumvent the use of diffraction to distinguish the phases [23]. It was shown that the oxygen ELNES of each phase had the same general shape, but significant differences were present in the locations and

intensities of the individual five peaks comprising the ELNES. Like the EELS spectra for the RE_2O_3 materials presented here, two peaks near the edge onset were the predominant features for the ZrO_2 samples. McComb found that the separation between these two peaks decreased slightly as cubic > tetragonal > monoclinic, similar to our findings. In the pure cubic phase of ZrO_2 there is only one type of coordination polyhedron around the Zr atom, ZrO_8, so the crystal field splitting is well defined, whereas the tetragonal structure has slightly distorted ZrO_8 polyhedra, the monoclinic structure has ZrO_7 polyhedra, and the stabilized cubic structure may have a mixture of polyhedra. Essentially, an increase in the complexity of the structure and coordination polyhedra around the metal ion results in variation of the initial oxygen 1s state as well as increased complexity in the splitting of the metal d orbital, so the peak separation of the O K ELNES is expected to decrease.

Specifically for RE_2O_3 materials, Brown *et al* [16] found that the oxygen K-edge ELNES is dependent on the crystal structure and that for the hexagonal phase the edge had a plateau followed by a second small peak; for the monoclinic phase, a round, broad peak was observed; and for the cubic phase there were two distinct peaks. They state that the difference in ELNES at the O K edge between the phases is not caused by crystal field effects since the oxygen atoms are located at sites with poorly defined symmetry. Brown *et al* suggest that the change in the environment around the oxygen atoms from one structure to another is enough to affect the Coulomb energy of the hole created by the impinging electron in the EELS process, and that this effect may create the difference in the O K-edge ELNES [16]. The observations of differences in the O K ELNES were noted again by Colliex *et al* [18]: the edge was characterized for all structures as having a main feature split into two peaks, with the cubic phase having the most distinct splitting, while the hexagonal and monoclinic structures presented weaker and irregularly shaped peaks. Although they did not present spectra from two crystal structures with the same chemical composition, the oxygen K ELNES of monoclinic Gd_2O_3 and cubic Yb_2O_3 match our results well. Furthermore, Colliex and Gasgnier stated that the three observed types of oxygen K-edge spectra (for the monoclinic and cubic phases as well as the hexagonal, which is not considered here) were reflective of the dipole-allowed transitions from the O 1s to the p partial density of states located above the Fermi level, which vary with the crystal structure [24].

The cubic structure of RE_2O_3 can be described as a fluorite unit cell doubled in size with one-quarter of the oxygen sites vacant. Around the RE cation, O anions are located at six of the eight corners of a cube, with the two remaining sites vacant, either along a face diagonal (type I) or a body diagonal (type II). Type I sites make up 75% of the total number. The actual positions of the oxygen atoms are not exactly at the cube corners, so a distorted octahedron is a more accurate description. The oxygen anions are all tetrahedrally coordinated by RE cations.

In the monoclinic structure—which, for the same composition, has a higher density and lower degree of symmetry than the cubic structure—the anion octahedron around the RE cation is further distorted and the oxygen coordination number of the RE cations becomes a mix of six and seven. There are three distinct cation crystal sites, and the coordination of the oxygen anions is significantly different from that of the cubic structure, having not only the tetrahedral arrangement of cations but also octahedral and square pyramidal [25]. However, three-fifths of the oxygen atoms are tetrahedrally coordinated, a substantial majority.

The bonding in RE_2O_3 is not purely ionic, and this degree of covalency allows for the mixing of the RE and O electronic states. It has been shown that while the RE 6s and 4f shells contribute to the overlap of RE orbitals with O 2p orbitals, this is dominated by the RE 5d shells [26, 27] so that the O 2p shell is not fully filled. According to crystal field theory, for an octahedrally coordinated metal atom (as is the case with all the RE atoms in the cubic phase

and with most in the monoclinic phase), the d orbitals will be split into a low-energy set of three orbitals, t_{2g}, and a higher energy pair, e_g [28]. The formation of molecular orbitals between the RE 5d orbitals and the O 2p means that some component of the t_{2g}–e_g splitting will be evident in the O 2p orbitals. The oxygen K edge observed in EELS is contributed to by the promotion of an O 1s core electron to a 2p vacancy according to the dipole selection rule ($\Delta l = \pm 1$), so the two ELNES peaks shown here and in many other oxides reflect the split 5d level. The double-peak structure in the oxygen K edge has been historically identified as the fingerprint of tetrahedrally coordinated oxygen atoms.

Since the majority of the oxygen atoms in the monoclinic phase are tetrahedrally coordinated, despite the distortion of the crystal structure relative to the cubic phase, it is not surprising that the O K ELNES has the double-peak structure. Following McComb's analysis summarized above, the decreased peak separation observed in the monoclinic REO-NPs relative to the cubic NPs is a result of the increased structural complexity, polyhedron variety, and reduced symmetry that all may affect the initial O 1s state as well as the splitting of the RE 5d level, which is hybridized with the final O 2p state.

The subtle decrease of the peak separation for each phase with decreasing atomic number (increasing ionic radius) is more difficult to explain. Ryzhkov *et al* [26, 27] have shown that the RE–O bond length affects the coupling of the O 2p to the RE 5d orbitals: a higher atomic number correlates to a shorter bond length, which increases the 2p–5d coupling. Also, Ishibashi *et al* [29] found that an increase in atomic number (RE = Y to Tm to Yb) decreases the mean ionic charge of the RE atom in the cubic phase RE_2O_3. Both of these findings may relate to a slight change in the energy difference between the t_{2g} and e_g levels, due either to closer packing of the atoms or a change in covalency, which would subsequently be expressed in the O K ELNES double-peak separation.

Other factors possibly contributing to the width and intensity of the oxygen ELNES include the spin–orbit splitting of the rare earth d electrons and the multiplet splitting of the rare earth d and f shells [22]. The theory invoked to create an accurate description of the RE_2O_3 O K-edge ELNES needs to be developed to describe in detail how the symmetry and coordination amongst the atoms creates the structure in the EELS spectra presented here.

5. Conclusion

Synthesis of heavy rare earth sesquioxide nanoparticles with gas-phase combustion produced nanoparticles from 20 to 50 nm in size and of two phases, cubic and monoclinic, depending on the temperature of the flame. EELS was used to investigate the oxygen K edge and the ELNES of this edge was shown to be a good fingerprint for the identification of the cubic versus the monoclinic structure. While both phases exhibited a double peak in the O K ELNES, the peaks overlap more in the case of the monoclinic phase. In general, for the heavy RE oxides studied here (Ho_2O_3 to Yb_2O_3) the peak separation is less for the monoclinic phase than the cubic, and the separation decreases slightly with increasing cation radius (decreasing atomic number). The theory behind the observed differences in ELNES of different structures is still indeterminate, and a thorough description of the molecular orbitals is required to fully explain the change in the ELNES between the cubic and monoclinic phases of the RE_2O_3.

Acknowledgments

Jacek Jasinski is gratefully acknowledged for his meaningful discussions pertaining to this work. The TEM work carried out here was performed at the National Center for Electron

Microscopy at the Lawrence Berkeley National Laboratory under US Department of Energy contract DE-AC-03-76SF00098, and the authors would like to thank the staff there, especially Tamara Radetic, for their assistance. This work was supported by NSF Advance Fellows Award No 0137922 and NSF NIRT Grant DBI-0102662.

References

[1] Que W, Zhou Y, Lam Y L, Pita K, Chan Y C and Kam C H 2001 *Appl. Phys.* A **73** 209–13
[2] Xu R, Zhu Y Y, Chen S, Xue F, Fan Y L, Yang X J and Jiang Z M 2005 *J. Cryst. Growth* **277** 496–501
[3] Mikelashvili V, Eisenstein G and Edelmann F 2002 *Appl. Phys. Lett.* **80** 2156–8
[4] Mekhemer G A H 2004 *Appl. Catal.* A **275** 1–7
[5] Yamamoto T, Matsuyama T, Tanaka T, Funabiki T and Yoshida S 2000 *J. Mol. Catal.* A **155** 43–58
[6] Hoekstra H R 1966 *Inorg. Chem.* **5** 754–7
[7] Guo B, Harvey A S, Risbud S H and Kennedy I M 2005 The formation of B-type monoclinic Y_2O_3 nanoparticles in a flame process *Phil. Mag.* submitted
[8] Egerton R F 1996 *Electron Energy-Loss Spectroscopy in the Electron Microscope* 2nd edn (New York: Plenum)
[9] Brydson R, Sauer H, Engel W, Thomas J M, Zeitler E, Kosugi N and Kuroda H 1989 *J. Phys.: Condens. Matter* **1** 797–812
[10] Grunes L A, Leapman R D, Wilker C N, Hoffmann R and Kunz A B 1982 *Phys. Rev.* B **25** 7157–73
[11] Paterson J H and Krivanek O L 1990 *Ultramicroscopy* **32** 319–25
[12] Xu F F and Bando Y 2001 *J. Appl. Phys.* **89** 5469–72
[13] Garvie L A J and Buseck P R 1999 *J. Phys. Chem. Solids* **60** 1943–7
[14] Gilliss S R, Bentley J and Carter C B 2005 *Appl. Surf. Sci.* **241** 61–7
[15] Manoubi T, Colliex C and Rez P 1990 *J. Electron. Spectrosc. Relat. Phenom.* **50** 1–18
[16] Brown L M, Colliex C and Gasgnier M 1984 *IXCOM Conf. (Toulouse, France)*; *J. Physique Coll.* **45** C2 433–6 (Les Editions de Physique)
[17] Fortner J A and Buck E C 1996 *Appl. Phys. Lett.* **68** 3817–9
[18] Colliex C, Manoubi T, Gasgnier M and Brown L M 1985 *Scanning Electron Microscopy II* ed O Jahari (Chicago, IL: SEM Inc.) pp 489–512
[19] Pearson D H, Fultz B and Ahn C C 1988 *Appl. Phys. Lett.* **53** 1405–7
[20] Ahn C C and Rez P 1985 *Ultramicroscopy* **17** 105–15
[21] Soldatov A V, Ivanchenko T S, Della Longa S, Kotani A, Iwamoto Y and Bianconi A 1994 *Phys. Rev.* B **50** 5074–80
[22] Jollet F, Petit T, Gota S, Thromat N, Gautier Soyer M and Pasturel A 1997 *J. Phys.: Condens. Matter* **9** 9393–401
[23] McComb D W 1996 *Phys. Rev.* B **54** 7094–120
[24] Colliex C and Gasgnier M 1984 *Physical Chemistry of the Solid State: Applications to Metals and Their Compounds: 37th Int. Mtg of the Societe de Chimie Physique (Paris, France)* ed P Lacombe (Amsterdam: Elsevier) pp 165–81
[25] Yakel H L 1979 *Acta Crystallogr.* B **35** 564–9
[26] Ryzhkov M V, Gubanov V A, Teterin Y A and Baev A S 1985 *Z. Phys.* B **59** 7–14
[27] Ryzhkov M V, Gubanov V A, Teterin Y A and Baev A S 1985 *Z. Phys.* B **59** 1–6
[28] Dunn T M, McClure D S and Pearson R G 1965 *Some Aspects of Crystal Field Theory* (New York: Harper and Row)
[29] Ishibashi H, Shimomoto K and Nakahigashi K 1994 *J. Phys. Chem. Solids* **55** 809–14